Chemistry & Biology
Brief Communication

A Nuclear-Localized Fluorescent Hydrogen Peroxide Probe for Monitoring Sirtuin-Mediated Oxidative Stress Responses In Vivo

Bryan C. Dickinson,[1,6] Yan Tang,[3,4,5,6] Zengyi Chang,[3,4,5,*] and Christopher J. Chang[1,2,*]
[1]Department of Chemistry, The University of California, Berkeley, CA 94720, USA
[2]Howard Hughes Medical Institute, Berkeley, CA 94720, USA
[3]State Key Laboratory of Protein and Plant Gene Research, Peking University, Beijing 100871, China
[4]School of Life Sciences
[5]Center for Protein Science
Peking University, Beijing 100871, China
[6]These authors contributed equally to this work
*Correspondence: chrischang@berkeley.edu (C.J.C.), changzy@pku.edu.cn (Z.C.)
DOI 10.1016/j.chembiol.2011.07.005

SUMMARY

Hydrogen peroxide (H_2O_2) can serve as a beneficial signaling agent or toxin depending on its concentration and location within a cell or organism. Methods to measure the localized accumulation of H_2O_2 in living specimens remain limited. Motivated to meet this need, we have developed a nuclear-localized fluorescent probe for H_2O_2, Nuclear Peroxy Emerald 1 (NucPE1), to selectively interrogate ROS fluxes within this sensitive organelle. NucPE1 selectively accumulates in the nuclei of a variety of mammalian cell lines as well as in whole model organisms like *Caenorhabditis elegans*, where it can respond to subcellular changes in H_2O_2 fluxes. Moreover, in vivo NucPE1 imaging reveals a reduction in nuclear H_2O_2 levels in worms overexpressing sir-2.1 compared with wild-type congeners, supporting a link between this longevity-promoting sirtuin protein and enhanced regulation of nuclear ROS pools.

INTRODUCTION

Reactive oxygen species (ROS) like hydrogen peroxide (H_2O_2) are endogenously produced metabolites that can be utilized at the cellular level for physiological processes ranging from growth to proliferation to migration (Bae et al., 1997; Niethammer et al., 2009; Paulsen and Carroll, 2010). However, in a larger context, aberrant ROS generation and/or accumulation at the organism level can result in the general phenomenon of oxidative stress, which is considered an inevitable consequence of aerobic life (Finkel et al., 2007; Frey et al., 2009; Murphy, 2009; Sundaresan et al., 1995) and forms the basis for the free radical theory of aging (Harman, 1956).

Recent data suggest that whether a particular ROS serves as a beneficial signaling agent or a toxic hazard depends on the specific identity of the ROS, the concentration of the ROS, and the subcellular localization of the generation and accumulation of the ROS (D'Autréaux and Toledano, 2007; Dickinson and Chang, 2011; Murphy et al., 2011). H_2O_2, in particular, has emerged as an ROS that can serve a variety of both helpful and harmful roles within the cell, depending on its location and concentration. To this end, mammalian cells have evolved exquisite mechanisms to regulate H_2O_2 fluxes. Included are colocalization of sources and targets, redox buffer control, and gatekeepers to H_2O_2 fluxes across the cell membrane (Miller et al., 2010; Woo et al., 2003, 2010; Wood et al., 2003). These discoveries highlight the importance of the subcellular location of H_2O_2 in determining the ultimate biological outcome of a redox encounter.

The common sites of H_2O_2 generation within a cell include NADPH oxidase (Nox) proteins at the cell membrane, the electron transport chain in the mitochondria, various oxidases in peroxisomes, and phagosomes in specialized cells of the immune system (Winterbourn, 2008). Each of these organelles has evolved efficient mechanisms to deal with the heightened redox load they must function under. Moreover, the natural turnover of proteins, nucleic acids, and lipids provides a mechanism to deal with irreversibly oxidized/damaged functionalities on each of these biomolecules. However, genomic DNA located within the nucleus can be irreversibly damaged and altered by rogue ROS. Over time, this stress can lead to the accumulation of ROS-mediated oxidative damage to genetic material that is connected to aging and diseases where age is a risk factor, including cancer and Alzheimer's disease (Bohr, 2002; Markesbery and Lovell, 2006).

Accordingly, new methods for directly and specifically monitoring changes in nuclear H_2O_2 fluxes offer a potentially powerful set of tools for probing the relationships between nuclear oxidative stress, aging, and disease states. Current methods for targeting H_2O_2-responsive imaging reporters to the nucleus rely on transfection (Malinouski et al., 2011; Mishina et al., 2011; Srikun et al., 2010), which varies in efficiency from cell type to cell type and is often technically difficult in whole animal specimens. Targeted small molecule fluorescent probes offer an enticing methodology for studying localized ROS fluxes, as we have recently demonstrated with a mitochondrial targeted H_2O_2 probe (Dickinson and Chang, 2008) and two different H_2O_2 probes with cytoplasmic trapping groups that resulted in enhanced H_2O_2 sensitivity within this locale (Dickinson et al.,

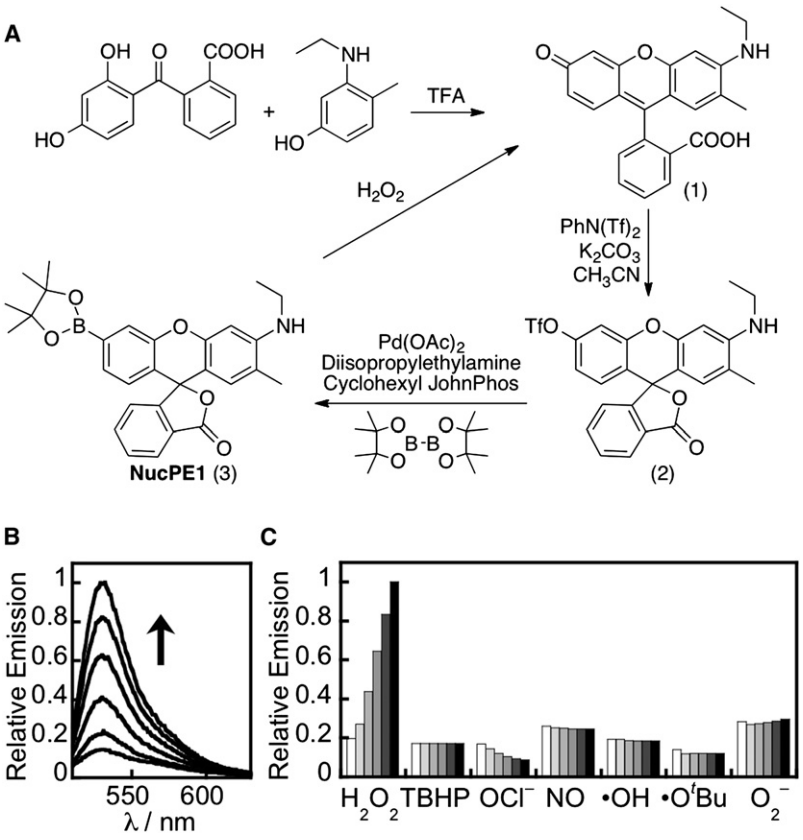

Figure 1. Synthesis and In Vitro Characterization of NucPE1

(A) Synthesis and activation of NucPE1.

(B) Fluorescence response of 5 μM NucPE1 to H_2O_2. Time points represent 0, 5, 15, 30, 45, and 60 min after the addition of 100 μM H_2O_2.

(C) Fluorescence responses of NucPE1 to various reactive oxygen species (ROS). Bars represent relative responses at 0, 5, 15, 30, 45, and 60 min after addition of each ROS.

2011; Miller et al., 2010). In this regard, nuclear-localized small-molecules remain rare (Dooley et al., 2004; Feng et al., 2010; Halvey et al., 2007; Koide et al., 2009; Mahon et al., 2007) and no examples reported to date are H_2O_2 responsive. Therefore, the identification of synthetic small molecule H_2O_2 indicators with inherent nuclear localization that work in living cells and animals would help elucidate the roles of nuclear ROS fluxes in a variety of biological processes. We now report the synthesis and application of a new first-generation chemical tool, Nuclear Peroxy Emerald 1 (NucPE1), to help meet this need.

RESULTS AND DISCUSSION

Synthesis and Characterization of NucPE1

Previous work from our laboratory has established the H_2O_2-mediated conversion of arylboronates to phenols as a general reaction-based strategy for selective and sensitive detection of cellular H_2O_2 in immune and neural signaling models (Albers et al., 2008; Chang et al., 2004; Miller et al., 2005, 2007; Srikun et al., 2010), but the vast majority of these probes do not possess a preferred subcellular localization. During the course of a systematic screen of rhodol platforms to develop a family of H_2O_2 indicators that span a wider color palette (Dickinson et al., 2010), we serendipitously discovered a boronate derivative that accumulates to the nuclei of live cells without the need for additional targeting groups. The synthetic route to this probe, NucPE1, is shown in Figure 1A. Condensation of 3-ethylamino-*p*-cresol and 2-(2,4-dihydroxybenzoyl)benzoic acid in TFA produces rhodol **1** in 67% yield. Treatment of **1** with *N*-phenyl bis(trifluoromethanesulfonamide) affords triflate **2** in 30% yield. Finally, palladium-mediated coupling with bis(pinacolato)diboron furnishes NucPE1 in 60% yield.

We evaluated the spectral characteristics and H_2O_2 response of NucPE1 in aqueous media buffered to physiological pH (20 mM HEPES, pH 7). NucPE1 features two major visible region absorptions (λ_{abs} = 468 nm, ε = 27,300 $M^{-1}cm^{-1}$; λ_{abs} = 490 nm, ε = 26,000 $M^{-1}cm^{-1}$) and a weak emission (λ_{em} = 530 nm, Φ = 0.117). Reaction of NucPE1 with H_2O_2 triggers a fluorescence increase upon its conversion to fluorophore **1**, which possesses one major absorption band at 505 nm (ε = 19,100 $M^{-1}cm^{-1}$) with enhanced emission (λ_{em} = 530 nm, Φ = 0.626). Kinetics measurements of the H_2O_2-mediated boronate deprotection were performed under pseudo-first-order conditions (5 μM dye, 10 mM H_2O_2), giving an observed rate constant of $k = 8.2 \times 10^{-3}$ s^{-1}. Figure 1B displays the H_2O_2-triggered fluorescence turn-on detected by NucPE1 over the course of 1 hr. As shown in Figure 1C, NucPE1 is selective for H_2O_2 over a panel of biologically relevant ROS, including superoxide, nitric oxide, and hydroxyl radical.

Validation of NucPE1 in Cell Culture

We next evaluated the subcellular distribution of NucPE1 in live mammalian cells. Confocal imaging of both HEK293 and HeLa cells loaded with NucPE1 and the nuclear stain Hoechst 33342 show good colocalization of the two dyes, establishing that NucPE1 accumulates specifically in the nucleus (Figure 2A). NucPE1 was then tested for its ability to respond to local changes in nuclear H_2O_2 levels. HEK293 cells loaded with NucPE1 and Hoescht 33342 and then washed and treated with 100 μM H_2O_2 exhibit marked increases in green NucPE1 fluorescence that maintains nuclear localization (Figures 2B and 2C). Similar results are observed in a wide variety of cell types, including HeLa, CHO.K1, NIH 3T3, Swiss 3T3, COS-7, A431, and Raw 264.7 Macrophages (see Figure S1 available online), demonstrating that NucPE1 can visualize changes in localized nuclear H_2O_2 pools in a range of mammalian cell systems. We note that the product compound **1** generated after peroxide cleavage does not localize to the nucleus of cells (Figure S1). This result establishes not only that the boronate moiety is required for this unexpected localization, but, more importantly, that any fluorescence change observed within the nucleus is due to nuclear H_2O_2 fluxes, because any NucPE1 deprotected outside of the nucleus will no longer localize to this organelle.

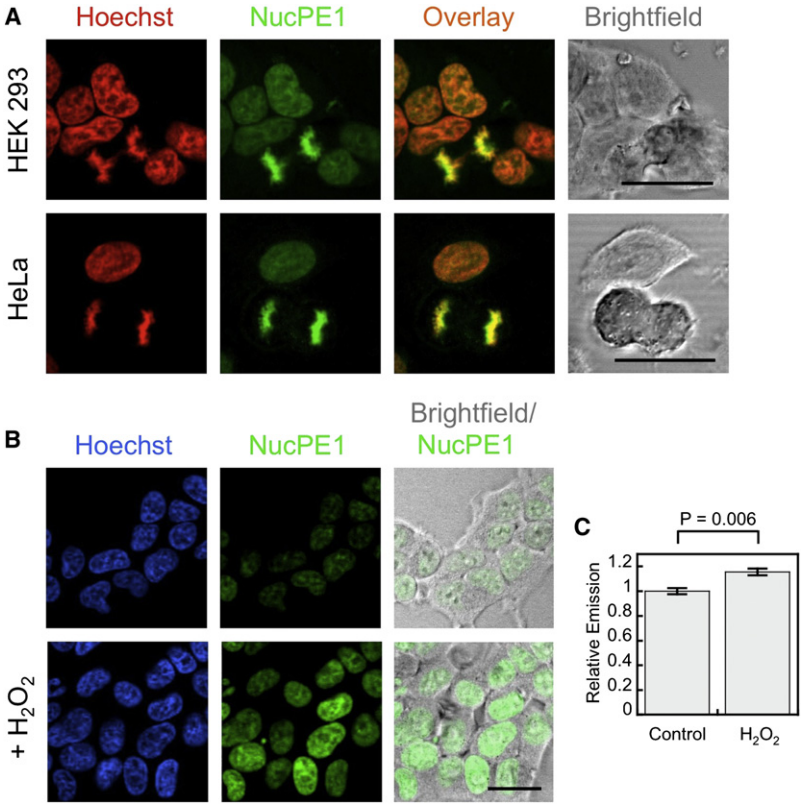

Figure 2. Localization and Turn-On of NucPE1 in Cell Culture

(A) HEK293 or HeLa cells loaded with 5 μM NucPE1 and 1 μM Hoechst 33342 for 15 min in DPBS, washed with DPBS, incubated 20 min in DPBS, and imaged. 25 μm scale bar shown.

(B) HEK293 cells loaded with 5 μM NucPE1 and 1 μM Hoechst 33342 for 15 min in DPBS, washed with DPBS, incubated 20 min in DPBS with carrier or 100 μM H_2O_2, and imaged. 20 μm scale bar shown.

(C) Quantification of NucPE1 fluorescence for experiment as shown in (B). Statistical analyses were performed with a Student's t test (n = 4) and error bars are ±SEM.

See also Figures S1 and S2.

We then performed several sets of experiments in an attempt to probe the origin of the observed nuclear localization of NucPE1. Initial studies focused on imaging mitotic cells stained with both NucPE1 and Hoescht 33342. Because this process involves breakdown of the nuclear envelope (Güttinger et al., 2009), we reasoned that if the nuclear localization of NucPE1 depends on active nuclear import, we would expect mitotic cells to no longer maintain colocalization between NucPE1 and Hoechst 33342, as the latter dye relies on DNA intercalation for its nuclear targeting. However, we observed that cells in late anaphase still show pronounced colocalization of NucPE1 and Hoechst 33342 (Figure 2A), suggesting that DNA is involved in the selective nuclear accumulation of NucPE1. However, our attempts to date to quantify this interaction in vitro by multiple methods, including monitoring absorption and emission changes, staining DNA gels with the NucPE1, or fluorescence polarization anisotropy measurements (Figure S2), have not revealed an unequivocal confirmation of DNA binding, which is still the most likely mode of localization as is observed in other nuclear staining fluorophores; the molecular mechanism of NucPE1 nuclear localization deserves future investigation. Nevertheless, NucPE1 selectively localizes to the nuclei of live mammalian cells, where it can respond to local changes in H_2O_2 levels.

Application of NucPE1 to Study H_2O_2 In Vivo

Organelle-localized ROS probes employed in vivo offer a powerful methodology to study organelle specific redox homeostasis in various physiological and pathological states, as was recently demonstrated by a mitochondrial targeted mass spectrometry H_2O_2 probe (Murphy et al., 2011). With the NucPE1 cellular results in hand, we sought to expand the scope and utility of this new probe by applying it to in vivo nuclear H_2O_2 imaging in the model organism *C. elegans*. Worms loaded with 150 μM Hoechst 33342 and 50 μM NucPE1 for 8 hr at 20°C and imaged by scanning confocal microscopy show tight colocalization between the two fluorophores throughout the worm (Figures 3A and 3B; Figure S3), confirming that NucPE1 maintains the ability to selectively target nuclei in vivo. We then used NucPE1 to interrogate nuclear redox responses to H_2O_2 in a *C. elegans* aging model. We focused our attention on Sir-2.1, an NAD-dependent histone deacetylase that when overexpressed can increase the lifespan of *C. elegans* and other model organisms (Chen and Guarente, 2007; Tissenbaum and Guarente, 2001). Interestingly, NucPE1 imaging of tail neurons in the wild-type control (N2) and Sir-2.1-overexpressing worms reveals a lower basal level of nuclear H_2O_2 in the latter, which exhibit the long-lived phenotype (Figure 4; Figure S4). Moreover, treatment with 10 mM H_2O_2 for 30 min causes a lower relative NucPE1 fluorescence increase for Sir-2.1-overexpressing *C. elegans* compared with wild-type counterparts (Figure 4; Figure S4), suggesting that these longer lived organisms possess enhanced nuclear protection against exogenous oxidative stressors. There could be differences in NucPE1 uptake, H_2O_2 permeability, and basal H_2O_2 levels between these genetic models. However, the differences between the basal NucPE1 signal and the oxidative stress fluorescent response are intriguing and should provide a basis for future studies.

SIGNIFICANCE

NucPE1 is a new type of H_2O_2-specific fluorescent probe that is specifically localized to cellular nuclei without appended targeting moieties, adding to the very short list of nuclear-localized fluorophores. NucPE1 is capable of visualizing local changes in H_2O_2 levels in a variety of common mammalian cell lines and in the model organism *C. elegans*. Moreover, this probe can detect differences in nuclear H_2O_2 levels and responses between wild-type *C. elegans* and ones that overexpress the longevity gene

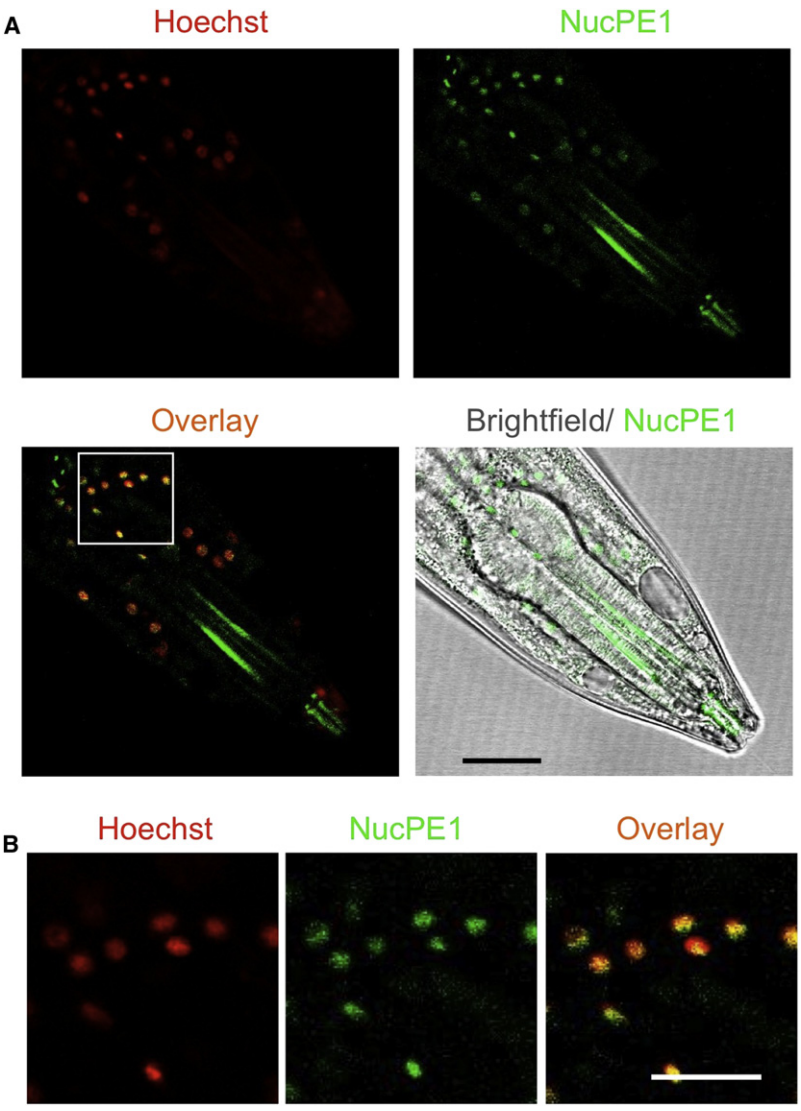

Figure 3. Localization of NucPE1 in *C. elegans*
(A) *C. elegans* loaded with 150 μM Hoechst 33342 and 50 μM NucPE1 for 8 hr and imaged. 20 μm scale bar shown. (B) The portion illustrated by a square in (A) is enlarged. 10 μm scale bar shown.
See also Figure S3.

Sir-2.1. NucPE1 and related chemical tools should prove very useful to further study the contributions of nuclear-localized H_2O_2 fluxes to healthy, aging, and disease states in a variety of biological models.

EXPERIMENTAL PROCEDURES

Synthesis of *N*-Ethyl (methyl) Rhodol (1)

3-Ethylamino-p-cresol (1.1 g, 7.0 mmol) and 2-(2,4-Dihydroxybenzoyl)benzoic acid (2.0 g, 7.7 mmol) were added to a heavy-walled pressure flask and dissolved in 10 ml of trifluoroacetic acid. The reaction contents were heated to 90°C for 24 hr. After cooling to room temperature, the contents were dried under reduced pressure. Purification by column chromatography (dichloromethane/10% methanol) yielded **1** as a red solid (1.7 g, 67%). ^{1}H NMR (CD_3OD, 400 MHz): δ 8.54 (1H, d, *J* = 7.6 Hz), 7.86 (1H, t, *J* = 7.6 Hz), 7.81 (1H. t, *J* = 7.6 Hz), 7.41 (1H, d, *J* = 6.8 Hz), 7.20 (1H, d, *J* = 9.2 Hz), 7.15 (1H, d, *J* = 2.4 Hz), 7.05 (1H, s), 7.02 (1H, s), 6.98 (1H, dd, *J* = 2.4, 9.2 Hz), 6.61 (2H, q, *J* = 7.2 Hz), 2.17 (3H, s), 1.35 (3H, t, *J* = 7.2 Hz). ^{13}C NMR (CD_3OD, 100 MHz): δ 166.8, 161.0, 159.3, 158.8, 156.5, 133.8, 132.5, 131.2, 130.8, 130.2, 129.9, 129.4, 128.0, 116.9, 115.7, 115.2, 101.7, 93.6, 38.4, 16.1, 12.5. LR-MS (ESI): calculated for [M^+] 374.4, found 373.9.

Synthesis of *N*-Ethyl (methyl) Rhodol Triflate (2)

Compound **1** (1.0 g, 2.7 mmol), *N*-phenyl bis(trifluoromethanesulfonamide) (1.9 g, 5.4 mmol), and potassium carbonate (1.5 g, 10.7 mmol) were added to a glass vial, dissolved in 5 ml of acetonitrile, and stirred at room temperature for 5 hr. The reaction contents were dried under reduced pressure. Purification by column chromatography (2:1 hexanes/ethyl acetate) yielded **2** as a faintly yellow solid (0.40 g, 30%). ^{1}H NMR ($CDCl_3$ /5% CD_3OD, 400 MHz): δ 8.01 (1H, d, *J* = 7.6 Hz), 7.67 (1H, t, *J* = 7.2 Hz), 7.62 (1H, t, *J* = 7.2 Hz), 7.19 (1H, d, *J* = 2.4 Hz), 7.15 (1H, d, *J* = 7.6 Hz), 6.88 (1H, dd, *J* = 2.0, 8.8 Hz), 6.83 (1H, d, *J* = 8.8 Hz), 6.39 (1H, s), 6.34 (1H, s), 3.19 (2H, q, *J* = 6.8 Hz), 1.92 (3H, s), 1.29 (3H, t, *J* = 6.8 Hz). ^{13}C NMR ($CDCl_3$ /5% CD_3OD, 100 MHz): δ 169.6, 152.7, 152.4, 150.8, 149.8, 148.7, 135.3, 130.0, 129.9, 128.1, 126.5, 125.1, 124.0, 119.9, 119.1, 116.0, 110.3, 104.5, 96.1, 83.1, 38.1, 16.7, 14.4. ^{19}F NMR ($CDCl_3$ /10% CD_3OD, 376.5 MHz): δ –71.995. LR-MS (ESI): calculated for [M^+] 506.5, found 505.5.

Synthesis of *N*-Ethyl (methyl) Rhodol Boronate, NucPE1 (3)

Compound **2** (150 mg, 0.30 mmol), bis(pinacolato)diboron (120 mg, 0.47 mmol), palladium acetate (63 mg, 0.10 mmol), and cyclo-hexyl JohnPhos (66 mg, 0.20 mmol) were added to a glass vial in an inert atmosphere glove box and dissolved in 3 ml of dioxane. Diisopropylethamine (0.31 ml, 1.79 mmol) was then added the vial and the contents stirred at room temperature overnight. The contents were then brought out of the box and dried under reduced pressure. Purification by column chromatography (1:1 hexanes/ethyl acetate) yielded **NucPE1** as a light orange solid (87 mg, 60%). ^{1}H NMR ($CDCl_3$/5% CD_3OD, 400 MHz): δ 8.00 (1H, d, *J* = 6.8 Hz), 7.68 (1H, s), 7.63 (1H, t, *J* = 8.0 Hz), 7.58 (1H, t, *J* = 7.2 Hz), 7.36 (1H, d, *J* = 8.0 Hz), 7.10 (1H, d, *J* = 7.2 Hz), 6.73 (1H, d, *J* = 7.6 Hz), 6.39 (1H, s), 6.35 (1H, s), 3.21 (2H, q, *J* = 7.2 Hz), 1.92 (3H, s), 1.26-1.33 (15H, m). ^{13}C NMR ($CDCl_3$ /5% CD_3OD, 100 MHz): δ 170.1, 153.6, 151.3, 151.0, 148.5, 135.0 129.5, 128.8, 128.2, 127.2, 126.5, 124.9, 123.9, 123.4, 121.6, 118.3, 105.1, 96.4, 84.2, 36.2, 24.7, 24.7, 16.7, 14.5. HR-FABMS: calculated for [M^+] 484.2290, found 484.2297.

Preparation and Staining of Cell Cultures

HEK293, HeLa, A431, NIH 3T3, Swiss 3T3, COS-7, and RAW264.7 macrophages were cultured in Dulbecco's Modified Eagle Medium (DMEM) containing high glucose with GlutaMAX (Invitrogen, Carlsbad, CA) and supplemented with 10% Fetal Bovine Serum (FBS, Hyclone). CHO.K1 cells were cultured in DMEM with F-12 supplements, glutamax (Invitrogen), and 5% fetal bovine serum (FBS, Hyclone). Two days before imaging, cells were passaged and plated on 18 mm glass coverslips. For all experiments, solutions of NucPE1 (from 5 mM stocks in DMSO) were made in DBPS with calcium chloride and magnesium chloride (Sigma). H_2O_2 was added by bath application to the medium from a 100 mM aqueous stock (Millipore H_2O). The cells were then kept in an incubator (37°C, 5% CO_2) during the course of all experiments.

Fluorescence Cell Imaging Experiments

Confocal fluorescence imaging studies were performed with a Zeiss LSM510 NLO Axiovert 200 laser scanning microscope and a 40× Achroplan IR

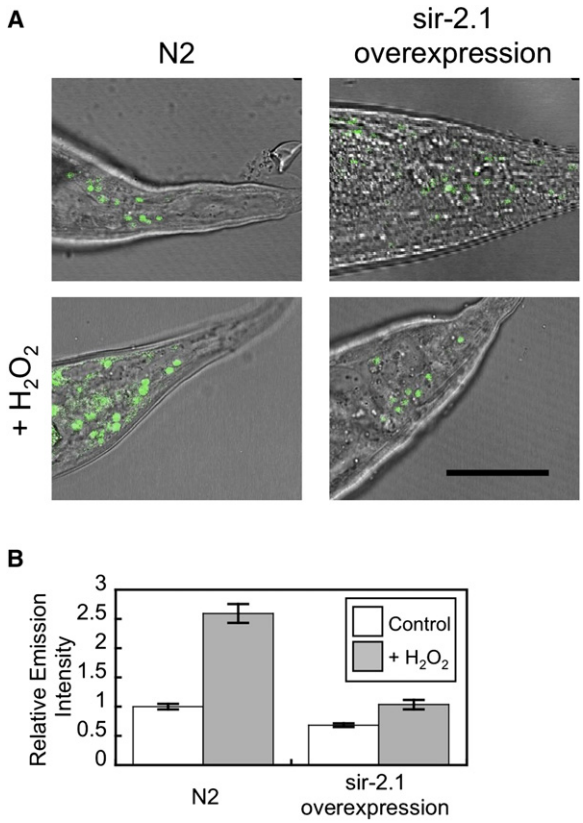

Figure 4. Sir-2.1 Overexpression Provides Nuclear Redox Protection
(A) Wild-type (N2) or Sir-2.1-overexpressing *C. elegans* loaded with 150 μM Hoechst 33342 and 50 μM NucPE1 for 8 hr, stimulated with either carrier or 10 mM H_2O_2 for 30 min, and imaged. Representative images of NucPE1 and a bright field overlay are displayed for one worm from each condition. 20 μm scale bar shown.
(B) Quantification of NucPE1 fluorescence for experiment as shown in (A). Error bars are ±SEM.
See also Figure S4.

water-immersion objective lens. Excitation of NucPE1-loaded cells at 514 nm was carried out with an Ar laser and emission was collected using a META detector between 522 and 554 nm. Excitation of Hoechst 33342 was carried out using a MaiTai two-photon laser at 780 nm pulses (mode-locked Ti:sapphire laser, Tsunami Spectra Physics) and emission was collected between 436 and 501 nm. All images in an experiment were collected simultaneously using identical microscope settings. Image analysis was performed in Image J. The background fluorescence was measured in a data set by selecting an ROI outside of the cells. This background number was then used to set the threshold of the image and thereby select for NucPE1 signal. The mean fluorescence intensity of this signal was then measured and utilized as the fluorescent signal for that particular image. The same threshold settings were utilized for all images in an experiment.

SUPPLEMENTAL INFORMATION

Supplemental Information includes four figures and Supplemental Experimental Procedures and can be found with this article online at doi:10.1016/j.chembiol.2011.07.005.

ACKNOWLEDGMENTS

This work was supported by the NIH (GM 79465 to C.J.C.), Amgen (C.J.C.), Astra Zeneca (C.J.C.), and Novartis (C.J.C.), NSFC CIHR (30711120582 to Z.C.), as well as National Key Basic Research Foundation of China (2006CB806508 and 2006CB910300 to Z.C.). C.J.C. is an Investigator with the Howard Hughes Medical Institute. We thank Holly Aaron (UCB Molecular Imaging Center) and Ann Fischer (UCB Tissue Culture Facility) for expert technical assistance. B.C.D. was partially supported by a Chemical Biology Interface Training Grant from the NIH (T32 GM066698).

Received: May 25, 2011
Revised: July 11, 2011
Accepted: July 13, 2011
Published: August 25, 2011

REFERENCES

Albers, A.E., Dickinson, B.C., Miller, E.W., and Chang, C.J. (2008). A red-emitting naphthofluorescein-based fluorescent probe for selective detection of hydrogen peroxide in living cells. Bioorg. Med. Chem. Lett. *18*, 5948–5950.

Bae, Y.S., Kang, S.W., Seo, M.S., Baines, I.C., Tekle, E., Chock, P.B., and Rhee, S.G. (1997). Epidermal growth factor (EGF)-induced generation of hydrogen peroxide. Role in EGF receptor-mediated tyrosine phosphorylation. J. Biol. Chem. *272*, 217–221.

Bohr, V.A. (2002). Repair of oxidative DNA damage in nuclear and mitochondrial DNA, and some changes with aging in mammalian cells. Free Radic. Biol. Med. *32*, 804–812.

Chang, M.C.Y., Pralle, A., Isacoff, E.Y., and Chang, C.J. (2004). A selective, cell-permeable optical probe for hydrogen peroxide in living cells. J. Am. Chem. Soc. *126*, 15392–15393.

Chen, D., and Guarente, L. (2007). SIR2: a potential target for calorie restriction mimetics. Trends Mol. Med. *13*, 64–71.

D'Autréaux, B., and Toledano, M.B. (2007). ROS as signalling molecules: mechanisms that generate specificity in ROS homeostasis. Nat. Rev. Mol. Cell Biol. *8*, 813–824.

Dickinson, B.C., and Chang, C.J. (2008). A targetable fluorescent probe for imaging hydrogen peroxide in the mitochondria of living cells. J. Am. Chem. Soc. *130*, 9638–9639.

Dickinson, B.C., and Chang, C.J. (2011). Chemistry and biology of reactive oxygen species in signaling or stress responses. Nat. Chem. Biol. *7*, 504–511.

Dickinson, B.C., Huynh, C., and Chang, C.J. (2010). A palette of fluorescent probes with varying emission colors for imaging hydrogen peroxide signaling in living cells. J. Am. Chem. Soc. *132*, 5906–5915.

Dickinson, B.C., Peltier, J., Stone, D., Schaffer, D.V., and Chang, C.J. (2011). Nox2 redox signaling maintains essential cell populations in the brain. Nat. Chem. Biol. *7*, 106–112.

Dooley, C.T., Dore, T.M., Hanson, G.T., Jackson, W.C., Remington, S.J., and Tsien, R.Y. (2004). Imaging dynamic redox changes in mammalian cells with green fluorescent protein indicators. J. Biol. Chem. *279*, 22284–22293.

Feng, S., Kim, Y.K., Yang, S., and Chang, Y.T. (2010). Discovery of a green DNA probe for live-cell imaging. Chem. Commun. (Camb.) *46*, 436–438.

Finkel, T., Serrano, M., and Blasco, M.A. (2007). The common biology of cancer and ageing. Nature *448*, 767–774.

Frey, R.S., Ushio-Fukai, M., and Malik, A.B. (2009). NADPH oxidase-dependent signaling in endothelial cells: role in physiology and pathophysiology. Antioxid. Redox Signal. *11*, 791–810.

Güttinger, S., Laurell, E., and Kutay, U. (2009). Orchestrating nuclear envelope disassembly and reassembly during mitosis. Nat. Rev. Mol. Cell Biol. *10*, 178–191.

Halvey, P.J., Hansen, J.M., Johnson, J.M., Go, Y.M., Samali, A., and Jones, D.P. (2007). Selective oxidative stress in cell nuclei by nuclear-targeted D-amino acid oxidase. Antioxid. Redox Signal. *9*, 807–816.

Harman, D. (1956). Aging: a theory based on free radical and radiation chemistry. J. Gerontol. *11*, 298–300.

Koide, Y., Urano, Y., Yatsushige, A., Hanaoka, K., Terai, T., and Nagano, T. (2009). Design and development of enzymatically activatable photosensitizer

based on unique characteristics of thiazole orange. J. Am. Chem. Soc. *131*, 6058–6059.

Mahon, K.P., Potocky, T.B., Blair, D., Roy, M.D., Stewart, K.M., Chiles, T.C., and Kelley, S.O. (2007). Deconvolution of the cellular oxidative stress response with organelle-specific Peptide conjugates. Chem. Biol. *14*, 923–930.

Malinouski, M., Zhou, Y., Belousov, V.V., Hatfield, D.L., and Gladyshev, V.N. (2011). Hydrogen peroxide probes directed to different cellular compartments. PLoS ONE *6*, e14564.

Markesbery, W.R., and Lovell, M.A. (2006). DNA oxidation in Alzheimer's disease. Antioxid. Redox Signal. *8*, 2039–2045.

Miller, E.W., Albers, A.E., Pralle, A., Isacoff, E.Y., and Chang, C.J. (2005). Boronate-based fluorescent probes for imaging cellular hydrogen peroxide. J. Am. Chem. Soc. *127*, 16652–16659.

Miller, E.W., Tulyathan, O., Isacoff, E.Y., and Chang, C.J. (2007). Molecular imaging of hydrogen peroxide produced for cell signaling. Nat. Chem. Biol. *3*, 263–267.

Miller, E.W., Dickinson, B.C., and Chang, C.J. (2010). Aquaporin-3 mediates hydrogen peroxide uptake to regulate downstream intracellular signaling. Proc. Natl. Acad. Sci. USA *107*, 15681–15686.

Mishina, N.M., Tyurin-Kuzmin, P.A., Markvicheva, K.N., Vorotnikov, A.V., Tkachuk, V.A., Laketa, V., Schultz, C., Lukyanov, S., and Belousov, V.V. (2011). Does cellular hydrogen peroxide diffuse or act locally? Antioxid. Redox Signal. *14*, 1–7.

Murphy, M.P. (2009). How mitochondria produce reactive oxygen species. Biochem. J. *417*, 1–13.

Murphy, M.P., Holmgren, A., Larsson, N.G., Halliwell, B., Chang, C.J., Kalyanaraman, B., Rhee, S.G., Thornalley, P.J., Partridge, L., Gems, D., et al. (2011). Unraveling the biological roles of reactive oxygen species. Cell Metab. *13*, 361–366.

Niethammer, P., Grabher, C., Look, A.T., and Mitchison, T.J. (2009). A tissue-scale gradient of hydrogen peroxide mediates rapid wound detection in zebrafish. Nature *459*, 996–999.

Paulsen, C.E., and Carroll, K.S. (2010). Orchestrating redox signaling networks through regulatory cysteine switches. ACS Chem. Biol. *5*, 47–62.

Srikun, D., Albers, A.E., Nam, C.I., Iavarone, A.T., and Chang, C.J. (2010). Organelle-targetable fluorescent probes for imaging hydrogen peroxide in living cells via SNAP-Tag protein labeling. J. Am. Chem. Soc. *132*, 4455–4465.

Sundaresan, M., Yu, Z.X., Ferrans, V.J., Irani, K., and Finkel, T. (1995). Requirement for generation of H2O2 for platelet-derived growth factor signal transduction. Science *270*, 296–299.

Tissenbaum, H.A., and Guarente, L. (2001). Increased dosage of a sir-2 gene extends lifespan in Caenorhabditis elegans. Nature *410*, 227–230.

Winterbourn, C.C. (2008). Reconciling the chemistry and biology of reactive oxygen species. Nat. Chem. Biol. *4*, 278–286.

Woo, H.A., Yim, S.H., Shin, D.H., Kang, D., Yu, D.Y., and Rhee, S.G. (2010). Inactivation of peroxiredoxin I by phosphorylation allows localized H(2)O(2) accumulation for cell signaling. Cell *140*, 517–528.

Woo, H.A., Chae, H.Z., Hwang, S.C., Yang, K.S., Kang, S.W., Kim, K., and Rhee, S.G. (2003). Reversing the inactivation of peroxiredoxins caused by cysteine sulfinic acid formation. Science *300*, 653–656.

Wood, Z.A., Poole, L.B., and Karplus, P.A. (2003). Peroxiredoxin evolution and the regulation of hydrogen peroxide signaling. Science *300*, 650–653.

